Article

Geochemical Characteristics of Geothermal Fluids of a Deep Ancient Buried Hill in the Xiong'an New Area of China

Mingxiao Yu [1,2], **Guiling Wang** [1,2,*], **Feng Ma** [1,2], **Wei Zhang** [1,2], **Wenjing Lin** [1,2], **Xi Zhu** [1,2] **and Hanxiong Zhang** [1,2]

1   Institute of Hydrogeology and Environmental Geology, Chinese Academy of Geological Sciences, Shijiazhuang 050061, China
2   Innovation Center of Geothermal and Dry Hot Rock Exploration and Development Technology, Ministry of Natural Resources, Shijiazhuang 050800, China
*   Correspondence: ihegwangguiling@sina.com

Abstract: The Xiong'an New Area is one of the areas with the richest geothermal resources in the east-central part of China. However, the genesis of the geothermal water in Jixianian carbonate reservoirs in this area is still unclear. This study conducted systematical geochemical and isotopic analyses of the geothermal water in the Jixianian carbonate reservoirs in the Rongcheng geothermal field and summed up the genetic mechanisms of geothermal fluids in deep geothermal reservoirs. The results are as follows: the geothermal water in the study area has a hydrochemical type of $Cl·HCO_3$-Na and originates from meteoric water in the Taihang Mountains. The age of the geothermal water increases from 22 ka in the west to 45 ka in the east, and its transport rate is approximately 1.02 m/a. The Sr concentration and $^{87}Sr/^{86}Sr$ ratio of the geothermal fluids increase along their runoff direction and are related to the dissolution and filtration of minerals such as dolomite and gypsum and the decay of ^{87}Rb in the Earth's crust. The geothermal water is involved in deep circulation and occurs in a closed system. These results are consistent with those obtained using the PHREEQC inverse model. The reverse hydrogeochemical simulation results exhibited the precipitation of gypsum and halite, the dissolution of anorthite and quartz, and desulfurization. The geothermal reservoir temperatures were estimated to be 92–113 °C using a SiO_2 geothermometer, and the thermal groundwater may have undergone deep circulation, with a prolonged retention time. Moreover, the groundwater occurs in a closed environment, strong water-rock interactions occur between the groundwater and related minerals, and the groundwater absorbs the heat from the deep heat source, thus forming geothermal water.

Keywords: Xiong'an New Area; Jixianian carbonate reservoir; hydrochemistry; water-rock interaction; geothermal fluids

1. Introduction

In the 21st century, mankind is faced with new challenges for sustainable development, such as energy shortage and environmental pollution. Countries all over the world have successively put peak carbon dioxide emissions and carbon neutrality on the agenda through legislation or planning and strategy formulation, which have become a new direction of green and low-carbon sustainable development. According to the latest energy statistics published by Our World in Data (2021a), geothermal energy, solar energy, water energy, wind energy, biomass energy, and ocean energy accounted for approximately 11.4% of the total global primary energy consumption in 2019 and are known as the six renewable energy sources in the world. Geothermal energy stored in the deep part of the Earth has large reserves and a low carbon footprint, and it is widely distributed and environmentally friendly. Moreover, it is easy to achieve the controllable sustainable exploitation of geothermal energy, thus providing a sustainable and stable energy supply [1,2]. As a national new district, the Xiong'an New

Area is one of the regions with the richest geothermal resources and the best development and utilization conditions in central and eastern China. To build this area into an eco-friendly city, it is necessary to study the deep hydrothermal process of geothermal fluids and focus on geothermal energy in the planning and construction of this area, achieve the goals of peak carbon dioxide emissions and carbon neutrality, and build a clean, low-carbon, reliable, and safe energy system.

At present, the main methods used to study the genesis and evolution of geothermal water include isotopic analysis, hydrogeochemistry, and hydrogeochemical simulation. Among them, stable isotope ratio analysis is widely employed to explain the origin and migration path of groundwater [3–7], and radioisotopes are widely used to determine the age of groundwater [8]. The study of the hydrochemical characteristics of geothermal fluids began in the 1950s. Many components and ion ratios can be used as tracers in the process of groundwater circulation and evolution, such as Cl^-, Br^-, I^-, and Sr^{2+} [9], as well as Ca/Cl, Mg/Cl, Ca/Sr, and Sr/^{87}Sr/^{86}Sr ratios [9,10]. In addition, the traditional hydrochemical analysis can be used to determine the possible water-rock interactions in the groundwater system based on hydrochemical data. However, it cannot quantify the water-rock interactions, which can be quantified through hydrogeochemical simulation. Scholars at home and abroad frequently study groundwater by simulating the reaction paths using the PHREEQC program, which can be used to investigate the formation, distribution, and evolutionary mechanisms of groundwater [11–13].

During the early 1990s and the 12th Five-Year Plan period, China conducted two detailed and systematic studies on geothermal resources in the North China Basin, summarizing the regional geothermal field characteristics and genetic models of geothermal resources and evaluating the potential of the geothermal resource in the basin [14,15]. In the Xiong'an new area, which lies in the North China Basin, the Ministry of Geology and Mineral Resources of China conducted many geological, hydrogeological, and geothermal surveys and evaluations and accumulated abundant hydrogeological and geothermal geological data. In recent years, many scholars have conducted in-depth research and discussions on the geothermal resources in this area [16–19]. The Rongcheng geothermal field is less geologically explored than the Niutuozhen geothermal field to the east. Therefore, the China Geological Survey has increased the exploration activities in the Rongcheng geothermal field since 2017, aiming to promote its development process. Previous studies on the geochemical characteristics of geothermal fluids in deep thermal storage in this area essentially focused on the geothermal reservoirs of the Jixianian Wumishan Formation [20,21]. By contrast, limited studies have been conducted on the geothermal reservoirs of the Gaoyuzhuang Formation—another main Jixianian thermal reservoir discovered in recent years—due to the karst characteristics of the reservoirs [22], leading to insufficient understanding of the occurrence environment and the migration and evolution patterns of the geothermal fluids in ancient buried-hill geothermal reservoirs. In addition, it is difficult to accurately identify the material sources and complex water-rock interactions of geothermal fluids only using traditional hydrochemical methods.

This study aims to (1) understand the hydrochemical characteristics of the geothermal water in the study area through the comprehensive analysis of geothermal water samples, (2) infer the origin of the geothermal water from the δ^2H–δ^{18}O isotopic composition of the geothermal water, spring water, and rainwater, (3) obtain the water age of the geothermal water based on the ^{13}C–^{14}C characteristics, (4) speculate the intensity of the water-rock interactions that the geothermal water has experienced by conducting Sr–^{87}Sr/^{86}Sr isotopic analysis and PHREEQC reverse simulation, and (5) determine the genetic mechanisms of the geothermal water in the study area by combining all the abovementioned results with the geological and structural evolution of the study area.

2. Geological Setting

The Xiong'an New Area lies in the central part of the Jizhong Depression in the Bohai Bay Basin (Figure 1a). It includes six fourth-order tectonic units: the Langfang depression,

the Niutuozhen uplift, the Baoding depression, the Gaoyang uplift, the Raoyang depression, and the Wuqing-Bazhou depression. The study area is located in the west-central part of the Xiong'an New Area and consists of the central portion of Rongcheng and the northern part of Anxin County. Regarding the tectonic location, the study area lies in the south of the Langfang depression in the Rongcheng uplift (Figure 1b), adjacent to the Niutuozhen uplift to the east and the Raoyang depression, the Gaoyang uplift, and the Baoding depression to the south [23]. The Rongcheng fault is a growth fault controlling the development of the Neoproterozoic strata and serves as the dividing line between the Niutuozhen uplift and the Rongcheng uplift. As a deep major fault active in a long term, the Xushui fault to the south was encountered by boreholes XR05 (D16) and XR21 (D19) and extends into the crystalline basement, acting as the dividing line between the Rongcheng uplift and the Baoding depression [21]. The Niudong fault, which is a syngenetic extensional fault, is the boundary between the Wuqing-Bazhou depression and the Niutuozhen uplift. As a deep major fault active in a long term, the Niunan fault, which is immediately south of the Niutuozhen uplift, is the normal fault controlling the southwestern boundary of the Niutuozhen uplift. These faults extend to different depths, and some of them even involve the crystalline basement, providing thermal and hydraulic conductivity channels for geothermal fluid transport (Figure 1c).

The strata in the study area mainly include Archean metamorphic rocks, Upper–Middle Proterozoic carbonate rocks, Ordovician–Cambrian limestones, Neogene breccias, and Quaternary sediments from bottom to top (Figure 2). The important target for geothermal resources exploration and development in this area is the carbonate reservoirs of the Jixianian Wumishan and Gaoyuzhuang formations, which are distributed throughout the study area. The deep carbonate strata have experienced erosion, weathering, and leaching for a long geological period and have well-developed dissolution vugs and fissures, which constitute storage space at favorable structural positions. The Jixianian geothermal reservoirs in the study area are characterized by a large water volume, high temperature, and strong rechargeability. The Jixianian strata have significantly different thicknesses on both sides of faults, which is small in uplifted parts and large on the flanks. According to the pumping test data of drilled boreholes, geothermal wells in the Wumishan Formation have a water yield of 60–200 m^3/h·m and a water temperature of 60–80 °C, and the geothermal wells in the Gaoyuzhuang Formation have a water yield of 50–170 m^3/h·m and a water temperature of 60–80 °C. Both the Wumishan and the Gaoyuzhuang Formations are marine strata mainly composed of carbonate rocks. They are thermal reservoirs featuring deep circulation and fractures and mainly comprise dolomite, quartz silica, and argillaceous dolomite. Their mineral components primarily include dolomite, calcite, gypsum, quartz, anorthite, halite, and illite.
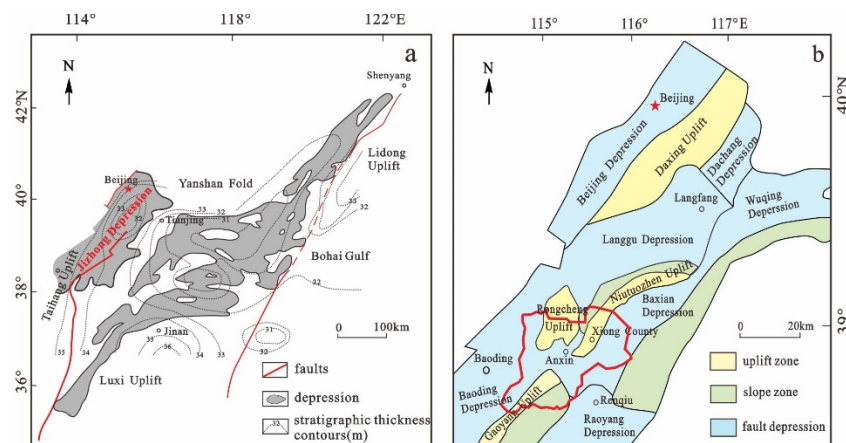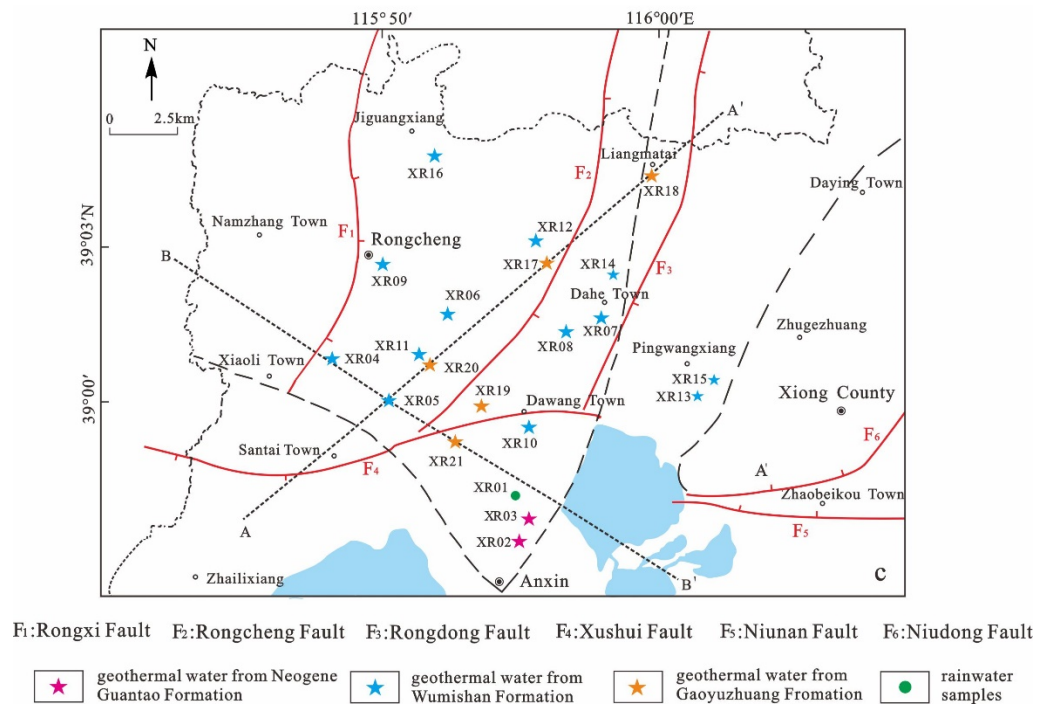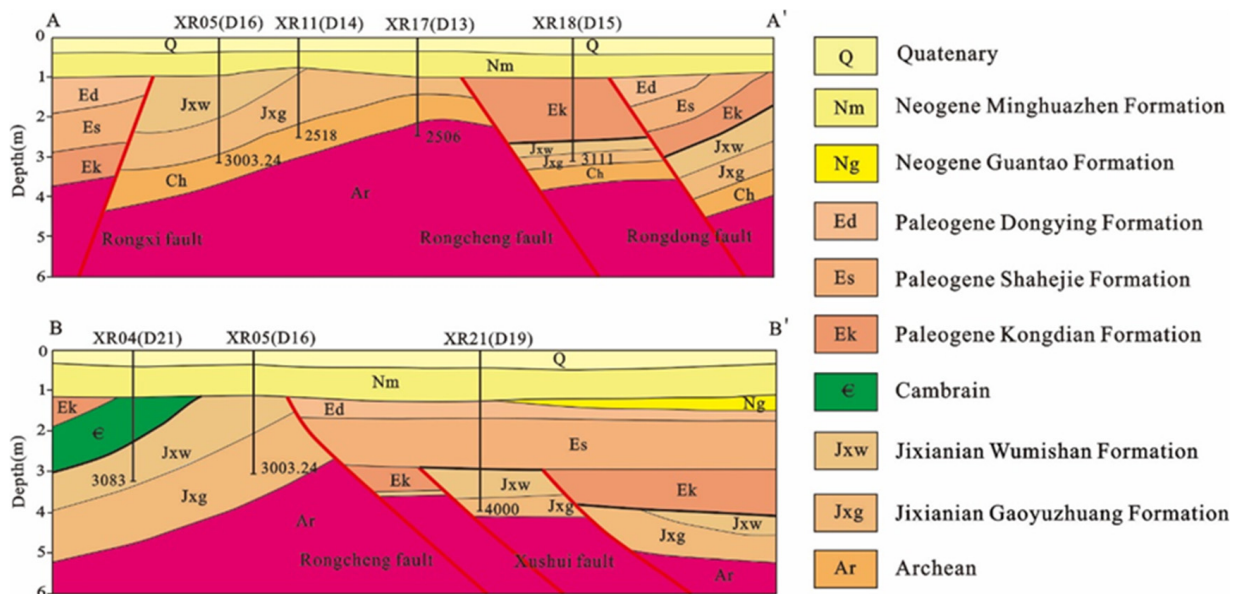

Figure 1. *Cont.*

Figure 1. (**a**) Basic tectonic map of the Bohai Bay Basin; (**b**) Basic tectonic map of the Jizhong depression; (**c**) Distributions of the major faults, geothermal fields, and boreholes in the Rongcheng [20,22].

Figure 2. Geological profiles of the study area. The locations of profiles (A-A′ and B-B′) refer to Figure 1c.

3. Methodology and Raw Data

In this study, 24 sets of water samples were collected from 2018 to 2020, including four sets of spring water samples from the Taihang Mountains area (T01–04), one set of rainwater samples from the Rongcheng geothermal field (XR01), three sets of geothermal water samples from the geothermal wells in the Neoproterozoic Guantao Formation (XR02–03), 12 sets of geothermal water samples from the geothermal wells in the Jixianian Wumishan Formation (XR04–16), and four sets of geothermal water samples from the geothermal well in the Gaizhuang Formation (XR16–21) (Figure 1c). While sampling, information such as geographical location, coordinates, and elevation were recorded, while the pH

and temperature on site were measured using portable thermometers. After rinsing twice using water from the sample source, all the geothermal water sample were filtered through 0.45 μm membranes and stored in three 200 mL polyethylene bottles. For H_2SiO_3 content analysis, the geothermal water samples were diluted by deionized water to 10% of their initial contents. With respect to metallic and cation elements analyses, samples were acidified to pH 1 with HNO_3.

The water samples were sent to the Key Laboratory of Groundwater Science and Engineering, Ministry of Land and Resources, using the Determination Method for Underground Water published by the Chinese government (DZ/T 0064-1993) [24]. The cation contents were detected using inductively coupled plasma analyses (ICAP6300), and the anion contents were measured using chromatography (ICS1500). The charge-balance error was <5%. The δ^2H and ^{18}O isotopic compositions were obtained using the isotope analyzer L2130i based on wavelength-scanned cavity ring-down spectroscopy technology. The analytical precision was $\pm 1‰$ for δ^2H and $\pm 0.1‰$ for $\delta^{18}O$. Carbon isotopes of the samples (XR04, 06, 07, 08, 09, 14, 15, and 17) were analyzed using the accelerator mass spectrometry (AMS) technique at the Beta Analysis Laboratory in Xiamen City, China, with analytical precision of $\pm 0.1‰$ for $\delta^{13}C$ and ± 0.1 pMC for ^{14}C. The $^{87}Sr/^{86}Sr$ ratios of the samples (XR04, 10, 13, 14, 15, 17, 18, and 20) were analyzed at the ultra-clean laboratory of the Zhongnan Mineral Resources Supervision and Testing Center, Ministry of Land and Resources. According to DZ/T 0184.19-1997 [25], Sr was separated and purified using the cation exchange method, and then the Sr isotopic composition was analyzed using a Triton thermal ionization mass spectrometer (00682T). To ensure the high accuracy, the test results were corrected according to the anion and cation milligram equivalent percentages of the water samples. The resulting data errors of the water samples were less than 5%, which was within the normal range. The test results are shown in Table 1.

During the runoff, geothermal water's hydrogeochemical composition changes with the reactions between the geothermal water and the surrounding rocks as minerals dissolve and precipitate [8,26]. The inverse hydrogeochemical simulation using the PHREEQC program is an effective tool to reflect the variations in water composition and water-rock interaction path [12]. By combining the reservoir minerals with hydrochemical composition of the geothermal water, the inverse model can be used to exhibit the mole transfer of major elemental ions and the behavior of the associated minerals [27]. This study constructed the inverse model using PHREEQC v3.6.2 (database: phreeqc.dat), and the flowchart is shown in Figure 3.
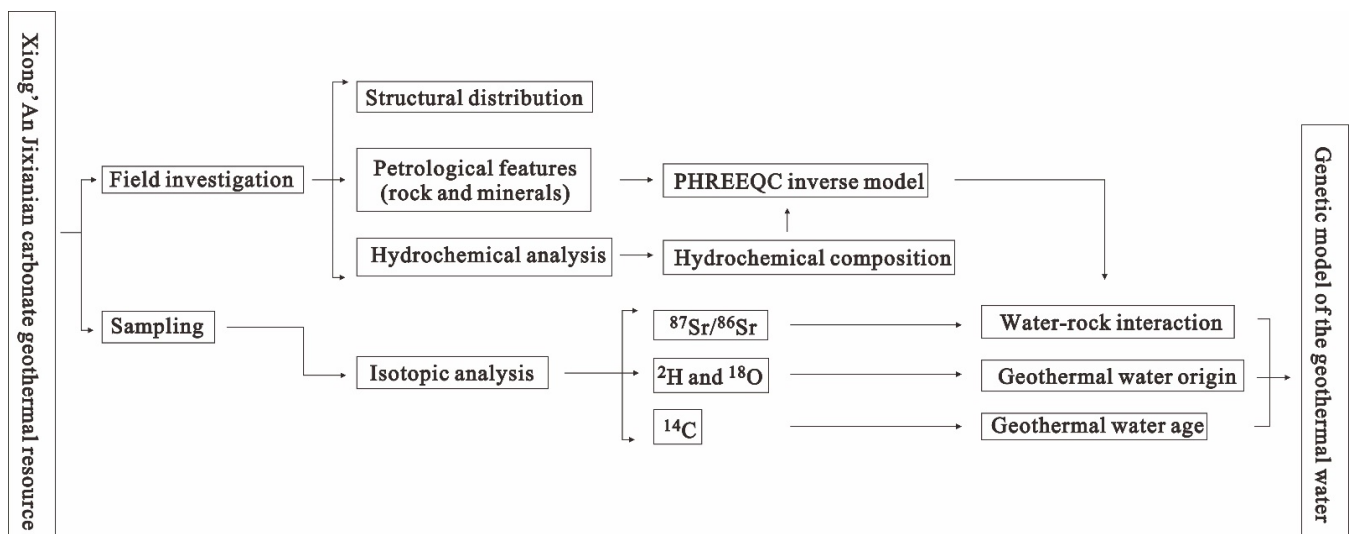

Figure 3. Flowchart of the research.

Table 1. Hydrochemical analysis data of the geothermal water from different aquifers in the study area and cold water from Taihang Mountains (mg/L).

Sample No.	Stratigraphic	T (°C)	pH	δ^2H (‰)	$\delta^{18}O$ (‰)	TDS	K^+	Na^+	Ca^{2+}	Mg^{2+}	HCO_3^-	Cl^-	SO_4^{2-}	H_2SiO_3	Sr^{2+}	$^{87}Sr/^{86}Sr(2s)$
T01 *	/	14	7.69	61.64	8.4	458	0.7	9	70.6	25.2	276.5	11.3	17.0	/	0.1	0.71153 ± 0.00005
T02 *	/	14	7.92	−67	−9.3	502	2.3	15.6	80.8	23.5	261.1	18.0	68.1	/	0.38	0.70926 ± 0.00002
T03 *	/	14	7.48	−74.09	−10.27	544	1.9	28.8	57.9	34.3	360.7	7.3	23.1	/	0.28	0.71051 ± 0.00004
T04 *	/	14	7.85	−75	−10.5	351	1.2	4.4	54.3	19.1	240.6	4.9	9.0	/	0.15	0.71070 ± 0.00003
XR01	/	/	7.15	−68	−9.4	27	0.2	0.6	2.4	0.1	17.9	1.7	1.6	/	0.01	/
XR02	Ng	42	8.63	−73.85	−9.91	1061	1.9	323	4.8	1.6	439.3	208.1	33.7	/	0.33	/
XR03	Ng	43	8.31	−75.71	−9.94	1193	2.1	371	5.3	1.5	447.3	308.7	18.7	/	0.37	/
XR04	Jxw	65	7	−74.14	−8.98	2784	42	833	53.1	24.4	669.7	1040	21.7	/	2.40	0.711525 ± 0.000008
XR05	Jxw	72	7.4	/	/	2787	43	783	55.4	28.9	704.3	1085	2.2	53.2	/	/
XR06 *	Jxw	55	6.94	−74.79	−8.66	2832	48	805	57.5	28.2	706.6	1101	1.2	51.6	2.92	0.71257 ± 0.00004
XR07 *	Jxw	68	7.17	−74.21	−8.57	2926	50	849	54.9	27.0	682.0	1164	8.7	65.3	2.70	0.71261 ± 0.00003
XR08 *	Jxw	71	7.31	−74.21	−8.64	2960	52	858	58.8	27.4	694.3	1175	1.6	62.1	2.88	0.71270 ± 0.00003
XR09 *	Jxw	55	7.2	−74.22	−8.72	2799	45	801	62.9	30.6	700.5	1079	<0.026	50.6	2.58	0.71187 ± 0.00001
XR10	Jxw	71	6.99	−75.12	−8.61	2908	53	835	53.8	23.9	662.4	1182	1.3	/	2.92	0.71265 ± 0.00002
XR11	Jxw	62	7.1	−75	−9	2914	47	827	62.6	32.0	735.0	1118	4.2	60.2	2.65	/
XR12	Jxw	56	8.18	−72.54	−8.62	2325	30	678	27.7	16.5	706.8	784	23.8	/	1.47	/
XR13	Jxw	70	6.98	−73.57	−8.86	2820	54	855	55.4	22.2	666.1	1080	1.6	/	2.88	0.712649 ± 0.000011
XR14	Jxw	71	8.63	−73.14	−8.61	2872	56	854	57.5	25.4	595.3	1136	3.1	/	2.92	0.712621 ± 0.000008
XR15	Jxw	/	7.27	/	/	2959	54	893	58.5	22.6	671.2	1167	2.5	67.1	2.70	0.71273 ± 0.00001
XR16	Jxw	71	7.32	/	/	2704	42	774	48.9	26.0	645.2	1076	4.1	60.3	2.51	/
XR17	Jxg	58	7.25	−73.89	−8.73	2809	46	815	59.3	26.5	701.7	1061	5.9	67.9	2.53	0.71209 ± 0.00004
XR18	Jxg	66	7.22	−74	−8.8	2901	49	828	61.0	31.3	705.9	1109	18.5	/	2.46	0.712504 ± 0.000008
XR19	Jxg	/	7.09	/	/	2927	48	858	62.6	26.7	687.1	1141	9.3	64.6	2.87	
XR20	Jxg	64	7.48	−75	−9	2620	44	721	59.2	30.4	703.5	985	4.3	68.3	2.41	0.71153 ± 0.00005
XR21	Jxg	/	7.99	/	/	2445	50	813	52.8	22.3	639.7	1068	11.4	82.8	0.38	/

Note: "*" indicates data collected from [21]. Ng denotes Neogene Guantao Formation; Jxw denotes Jixianian Wumishan Formation; Jxg denotes Jixianian Gaoyuzhuang Formation.

4. Results and Discussion

4.1. Hydrochemical Characteristics

In this study, the water samples for hydrochemical analysis were collected from spring water in the Taihang Mountains, rainwater in the Rongcheng geothermal field, and geothermal water in the Guantao, Wumishan, and Gaoyuzhuang Formations. According to the results of the hydrochemical compositional analysis (Table 1) and Piper diagram (Figure 4), the spring water samples collected from the area of exposed carbonate rocks in the Taihang Mountains (T01–04) had an average temperature of 14 °C, pH of 7.48–7.92, and TDS content of 458–544.1 mg/L, thus belonging to fresh water. Their main cations included Ca^{2+} and Mg^{2+}, their anions were HCO_3^-, and they had a hydrochemical type of HCO_3-Ca·Mg. The geothermal water samples from the Guantao Formation in the Rongcheng geothermal field (XR02–03) had a wellhead temperature of 42–43 °C, pH of 8.31–8.63, a hydrochemical type of Cl·HCO_3-Na, and TDS content of 1061–1193 mg/L. The geothermal water samples from the Jixianian carbonate reservoirs (XR04–21) had a wellhead temperature of 55–72 °C and pH of 7.04–8.18, indicating weakly alkaline water. Moreover, they had a TDS content of 2445–2960 mg/L and, thus, had the characteristic of brackish water. Their main cations were Na^+, which accounted for more than 80% of their total cations and had an average concentration of 677.8–893.7 mg/L. Their main anions included Cl^- and HCO_3^-; thus, they had a hydrochemical type of Cl·HCO_3-Na. According to the test results, the contents of chemical components and TDS content of the surface spring water samples from the Taihang Mountains area, the geothermal water samples from the Guantao Formation, and geothermal water samples from the Jixianian carbonate reservoirs (Jixianian Wumishan and Gaoyuzhuang formations) increased in turn (Figure 5), indicating that the leaching of the surrounding rocks is the material source of the geothermal water components. Moreover, the Jixianian carbonate reservoir system has a long circulation path, a closed storage space, and intense water-rock interactions between the geothermal water and the surrounding rocks.
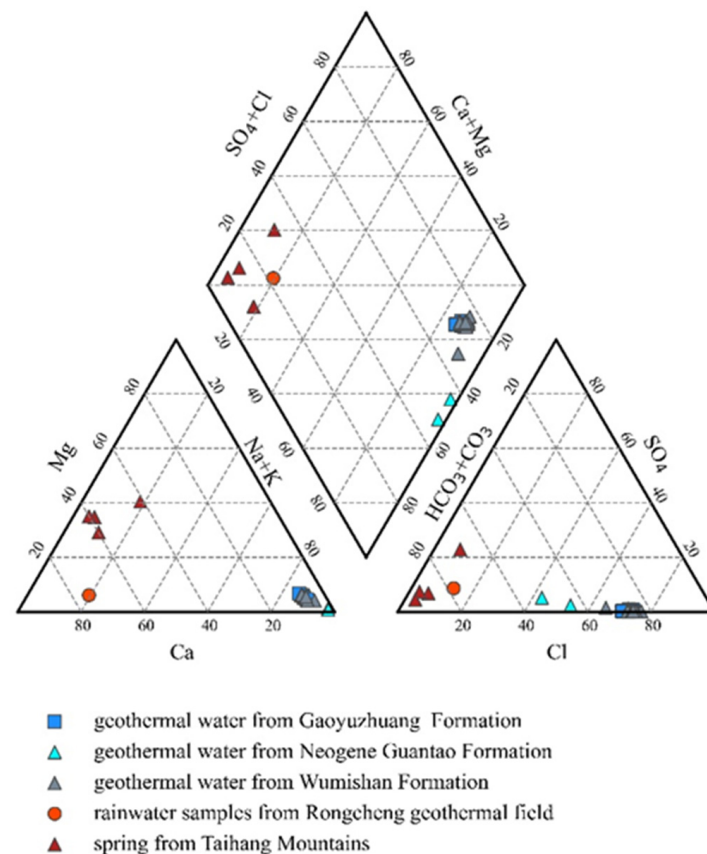
Figure 4. Piper diagram of the study area.
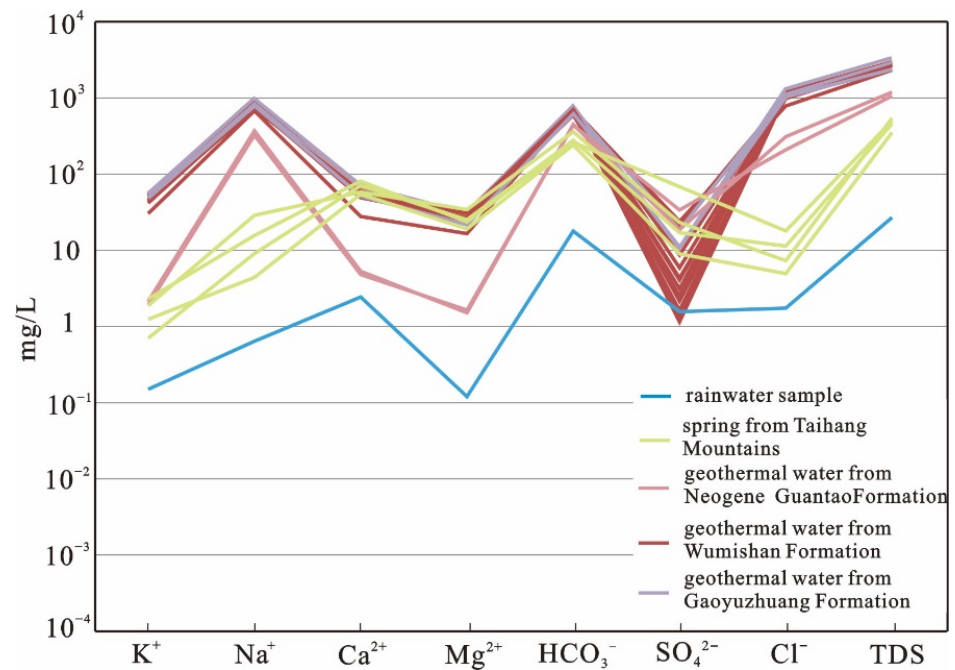
Figure 5. Schoeller diagram showing the water composition of the study area.

4.2. Isotopic Characteristics

4.2.1. H and O Isotopes

According to the global meteoric water line (GMWL) [28] and local meteoric water line (LMWL) [20], the relationship between the δ^2H and $\delta^{18}O$ values of different water bodies in the study area is plotted in Figure 6a. According to this figure, the water samples from different regions and thermal reservoirs are distributed on the meteoric water lines, indicating that the recharge source of the various water bodies in this area is precipitation.
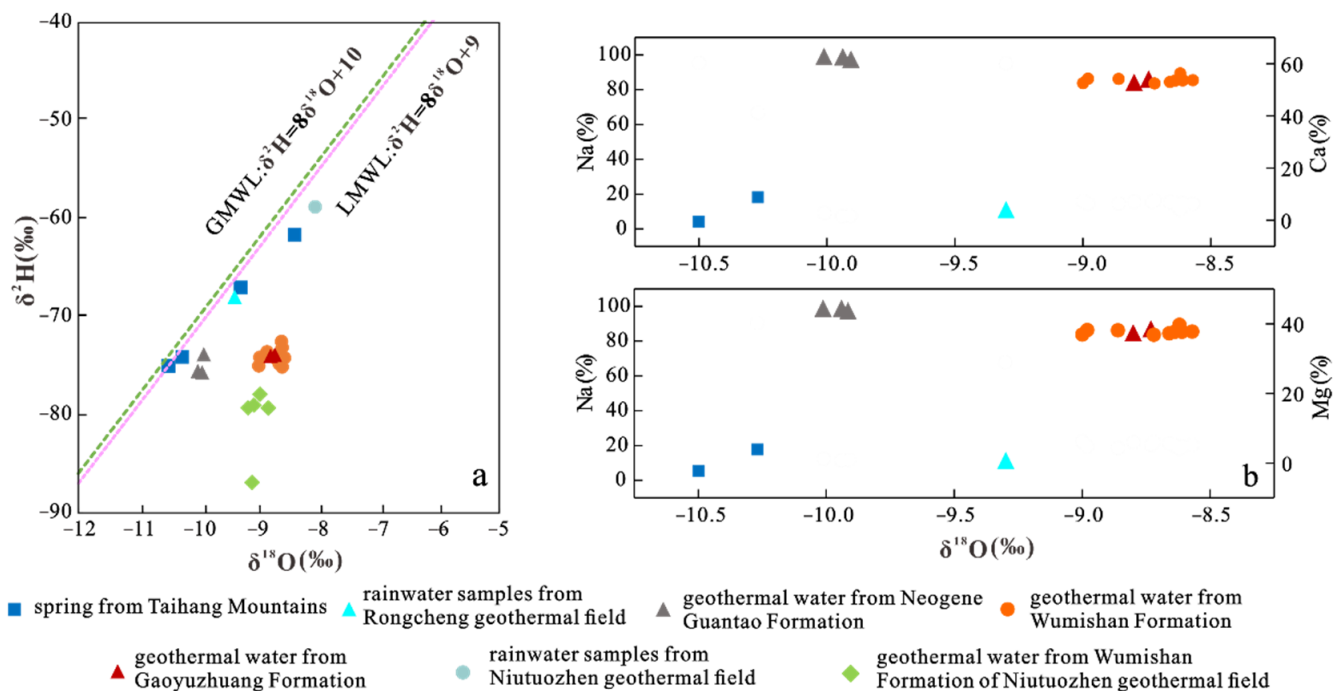
Figure 6. Plot of δ^2H–$\delta^{18}O$ (**a**) and $\delta^{18}O$–major ions (**b**) of water samples of the study area.

As shown in Figure 6b, different water-rock interaction processes lead to different distribution patterns of the data points of groundwater samples originating from atmospheric precipitation and can be used to reflect the changes in the hydrochemical type of the samples. The spring water samples from the Taihang Mountains area had $\delta^{18}O$ values less than $-9‰$, high Ca^{2+} and Mg^{2+} millimole fractions, a low Na^+ concentration, and a hydrochemical type of HCO_3-Ca·Mg. The area of exposed carbonate in the Taihang Mountains is more open and has quick water circulation. The geothermal water in this area is directly recharged by atmospheric precipitation and affected by evaporation and has a short circulation path. Moreover, the geothermal water in this area features a low degree of filtration and insignificant water-rock interactions. The geothermal water samples from the reservoirs of the Wumishan Formation had higher $\delta^{18}O$ values (greater than $-9‰$) than those from the deep Jixianian Gaoyuzhuang reservoirs in the study area. Moreover, they had a Na^+ millimole fraction more than 80%, Ca^{2+} and Mg^{2+} millimole fractions decreasing to less than 10%, and a chemical type of $Cl·HCO_3$-Na. Regionally, the deep carbonate reservoirs have rich geothermal water in some portions of the basin after being recharged by precipitation in the carbonate outcrops of the Taihang Mountains in the west and northwest and undergoing long-distance deep circulation and migration. As for the geothermal fluids in the study area, their hydrochemical type changes from HCO_3-Ca·Mg to Cl-HCO_3-Na, their salinity increases, and their water-rock interactions become stronger from northwest to southeast. Compared with the shallower Guantao Formation, the geothermal water samples from the sandstone geothermal reservoirs deviated from the meteoric water lines in the vertical direction and showed significant oxygen drift, indicating that the geothermal water in the carbonate reservoirs occurs in a closed environment and that the oxygen isotopic exchange with the surrounding rocks causes heavy isotope enrichment of the water.

In addition, Dansgaard [29] put forward the concept of the deuterium excess parameter ($d = \delta^2H - 8\delta^{18}O$), which can be used to study underground hot-water circulation. By comparison with the water samples from the Wumishan Formation in Niutuo Town in the adjacent area, the hot-water samples from the carbonate geothermal reservoirs in the study area had smaller d values. This result indicates that the portions with a large burial depth and hot water in the carbonate geothermal reservoirs feature more significant isotopic exchange.

4.2.2. C Isotopes

^{14}C is a major radioactive carbon isotope, and the quantification of geothermal water retention time by ^{14}C dating is the most simple and reliable method used to determine the age of groundwater [30]. ^{14}C dating is based on the measurement of the reduction in the radioactive parent nuclei (^{14}C) in a sample. The essence of ^{14}C dating is to determine the age of dissolved inorganic carbon in water rather than the age of water [10]. Therefore, it is necessary to determine the carbon sources when ^{14}C dating is used to determine the age of groundwater.

On the basis of the $\delta^{13}C$ values of different sources, the source and migration of carbon in groundwater can be traced. The inorganic carbon in groundwater is mainly derived from HCO_3^- formed by the dissolution of external CO_2 and carbonate rocks, and the external CO_2 mainly originates from atmospheric input, soils, and deep Earth. According to Mauna Loa Observatory in Hawaii, the highest CO_2 concentration in the atmosphere is no more than 410 µg/g. The content of inorganic carbon dissolved in rainwater is very low; thus, the influence of atmospheric CO_2 on the inorganic carbon in underground hot water can be ignored. Since there is no tectonic activity (e.g., magmatic intrusion and volcanic activity) in the study area, the CO_2 input from deep rock structural faults was not considered in this study. Dissolved carbonate rocks generally have $\delta^{13}C$ values of 0‰, while CO_2 in soils has a $\delta^{13}C$ value of approximately $-23‰$ [5]. The geothermal fluids in the deep thermal reservoirs of the study area had $\delta^{13}C$ values of $-16.6‰$ to $-2.2‰$, indicating that the ^{13}C of the geothermal water originates from both soils and carbonate rocks.

Overall, the dissolved inorganic carbon in the geothermal fluids of the Jixianian carbonate reservoirs mainly originates from the balanced CO_2 in soils and the carbon from carbonate rocks. Considering the effects of the source of dissolved inorganic carbon in the geothermal fluids on the ^{14}C dating of geothermal water, this study calculated the age of the hot groundwater in the study area using the groundwater dating decay equation corrected with the Pearson model [31]:

$$t = \frac{1}{\lambda} \ln \frac{qA_0}{A_t} = 8267 \ln \frac{qA_0}{A_t}, \tag{1}$$

$$q = \delta^{13}C_{DIC} - \delta^{13}C_{carb} \Big/ \delta^{13}C_{soil} - \delta^{13}C_{carb}, \tag{2}$$

where t is the apparent age of hot groundwater (a), λ is the decay constant of ^{14}C (12.1×10^{-6}), $\delta^{13}C_{DIC}$ is the $\delta^{13}C$ value of groundwater, $\delta^{13}C_{soil}$ is the $\delta^{13}C$ value of CO_2 in soil ($-23‰$), $\delta^{13}C_{carb}$ is the $\delta^{13}C$ value of carbon from carbonate rocks ($0‰$), A_0 is the initial radioactivity concentration of parent nucleus (100 pMC), and A_t is the radioactive ^{14}C concentration in groundwater.

The age of geothermal water in deep carbonate reservoirs in the study area was estimated to be 20–41 ka (Table 2). The corrected ages of geothermal water samples from well XR04 in the west and well XR15 in the east were 21 ka and 42 ka, respectively. Therefore, the geothermal water in the Rongcheng Uplift has a significantly smaller age than that in the Wacao area of Dahe Town in the east. In the Rongcheng geothermal field, the geothermal fluids from the Jixianian carbonate reservoirs at the locations of wells XR04 to XR15 have a flow migration rate of approximately 1.02 m/a, and they circulate slowly from west to east.

Table 2. ^{14}C corrected model age of geothermal water in the study area.

Sample No.	Zoning	^{14}C (pMC)	^{13}C (‰)	Pearson Model Corrected Age (ka)
XR04	Uplift	2.41	−6.2	20
XR06	Uplift	<0.44	−3.5	35
XR07	Uplift	<0.44	−3.8	36
XR08	Uplift	<0.44	−3.4	35
XR09	Uplift	1.1	−7.5	28
XR14	Uplift	<0.44	−2.8	33
XR17	Uplift	1.3	−3.8	21
XR15	Wacao area	0.5	−16.6	41

4.2.3. Sr Isotopes

Sr does not show any significant fractionation in natural processes and is not affected by evaporation and other processes. Presently, many scholars use Sr to study and solve the practical problems related to underground hot water [32,33]. The cold-water samples from the Taihang Mountains area had Sr concentrations of 0.1–0.378 mg/L and $^{87}Sr/^{86}Sr$ ratios of 0.7105–0.71153. The geothermal fluid samples from the Jixianian carbonate reservoirs in the study area had high Sr concentrations of 1.466–2.922 mg/L and $^{87}Sr/^{86}Sr$ ratios of 0.7115–0.7126. The Sr concentration in atmospheric precipitation is generally very low (the local rainwater samples collected in this study had a Sr concentration of 0.006 mg/L), and the Sr concentration in groundwater largely depends on the water-rock interactions between groundwater and water-bearing media [29]. The Sr in groundwater mainly originates from wind-carried sediments, minerals in weathering products (e.g., silicate, carbonate, and sulfate in soils), and water-bearing media. The $^{87}Sr/^{86}Sr$ ratios of the water samples were compared with those of carbonate sources (0.7088) and aluminum-silicate sources (0.7160–0.7200; Figure 7a) [34,35]. As revealed by the comparison results, the cold-water samples from the carbonate outcrops of the Taihang Mountains had similar $^{87}Sr/^{86}Sr$ ratios to the weathering source of carbonate rocks. However, there was a poor correlation between the TDS content and Sr^{2+} and Ca^{2+} concentrations, and the Sr in groundwater

may originate from the dissolution of Sr in carbonate rocks. The $^{87}Sr/^{86}Sr$ ratios of the geothermal fluid samples from the Jixianian carbonate reservoirs in the study area were higher than those of the carbonate source but lower than those of the aluminosilicate source. By combining the positive linear relationships between the TDS content and Sr^{2+} and Ca^{2+} concentrations (Figure 7b,c) as well as the lithologic composition of water-bearing media, it can be concluded that the Sr concentration in the geothermal fluids of the Jixianian carbonate reservoirs may be related to the filtration of Ca-bearing minerals (e.g., carbonates), which is further discussed below.
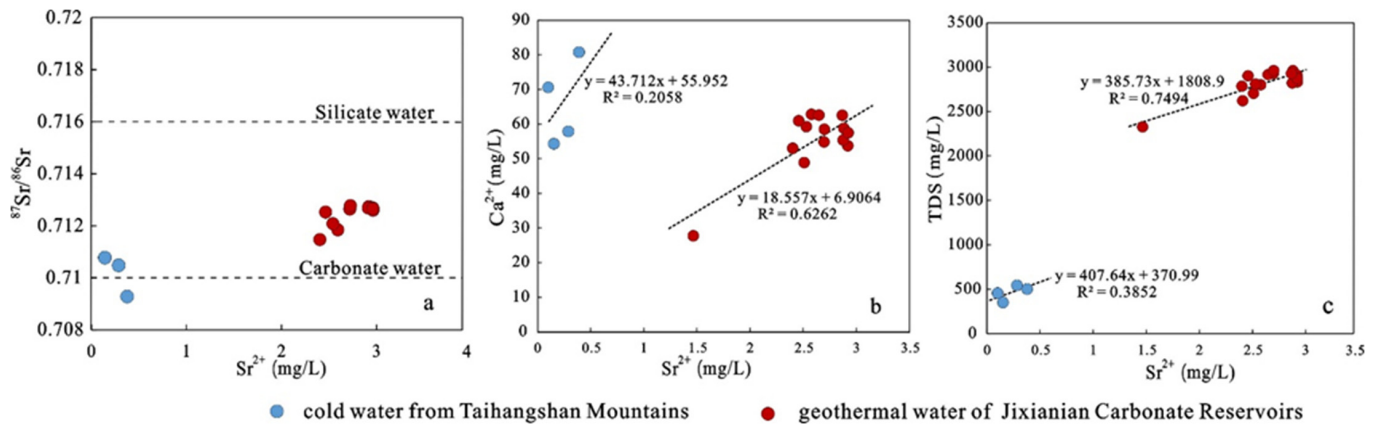
Figure 7. Plots of Sr versus $^{87}Sr/^{86}Sr$ ratio (**a**), Ca^{2+} (**b**), and TDS (**c**) content of the water samples.

The relationship between the Sr/Ca and $^{87}Sr/^{86}Sr$ ratios and the relationship between the $\delta^{18}O$ values and the $^{87}Sr/^{86}Sr$ ratio indicate the enrichment process of Sr isotopes from northwest to southeast and from the Taihang Mountains area to the water sampling points near the Rongxi fault zone and to the water sampling points near the Rongdong fault zone (Figure 8). During the long evolution of the crust, ^{87}Rb decayed into the radioactive element ^{87}Sr through β decay. With the decay of ^{87}Rb, the ^{87}Sr concentration in Rb-bearing rocks (gneiss) and minerals (muscovite) increases continuously as a function of time, showing the cumulative effect of time. The contour maps of the Sr concentration and $^{87}Sr/^{86}Sr$ ratio of the geothermal water of the Jixianian strata in the study area were plotted as a function of the accumulation effect of Sr isotope age and the characteristics of the groundwater hydrodynamic field (Figure 9a,b). They show a consistent upward trend from northwest to southeast.
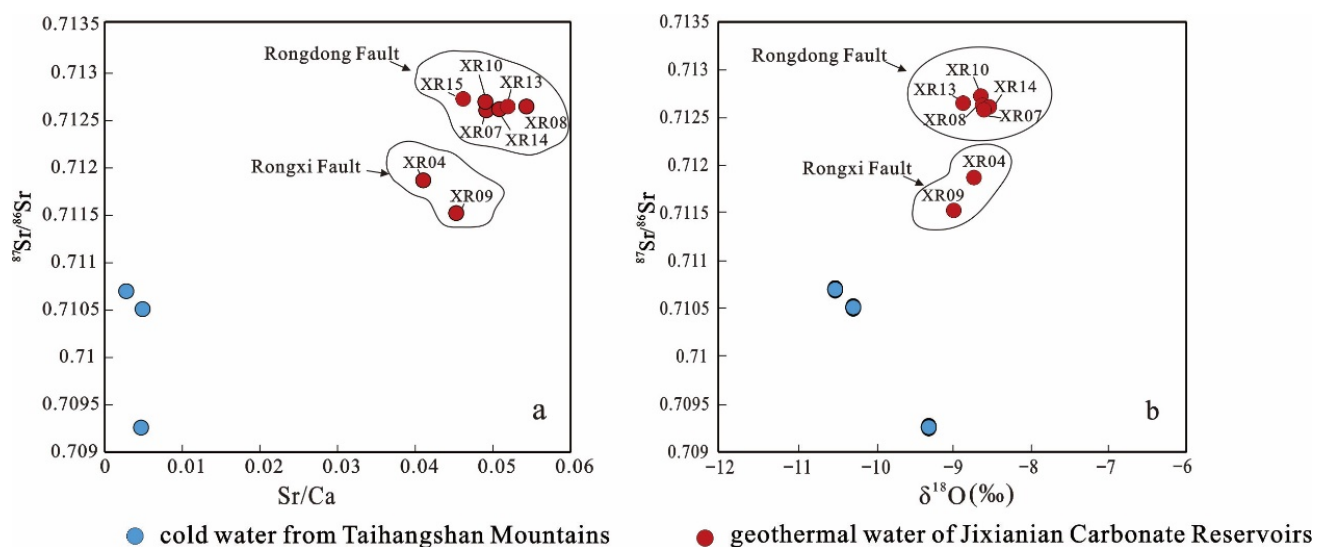
Figure 8. Plots of the Sr/Ca-$^{87}Sr/^{86}Sr$ (**a**) and $\delta^{18}O$–$^{87}Sr/^{86}Sr$ ratios (**b**) of the water samples.

Figure 9. Contour map showing the distribution of the Sr^{2+} content (**a**) and $^{87}Sr/^{86}Sr$ ratios (**b**) of the water samples from the Jixianian carbonate reservoirs.

4.2.4. PHREEQC Inverse Model

To determine the water–mineral reactions of a range of groundwater from that with simple composition and short-path circulation to that with complex composition and longer-path circulation, this study adopted the PHREEQC software to c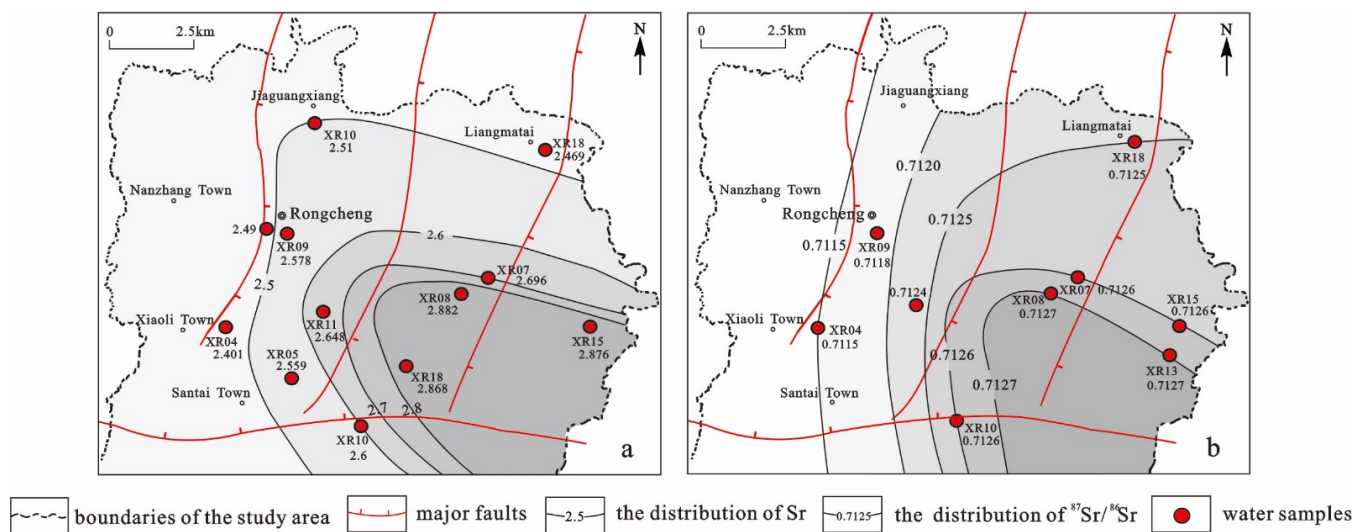onduct inverse simulations of the mineral dissolution and precipitation reactions in the underground hot water of the deep carbonate reservoirs in the study area [8]. During the simulations, the starting point of the water flow path was set to the sampling point (T01) of cold spring water in the Taihang Mountains area, and its endpoint was set to the sampling point (XR08) of the geothermal well of the Jixianian thermal reservoirs in the Rongcheng geothermal field at a low altitude. As demonstrated in Section 2, the reservoir minerals in the study area mainly include dolomite, calcite, gypsum, quartz, anorthite, halite, and illite. Considering the cation exchange and adsorption during the formation of spring water, CaX_2 was added to the model as an exchange reaction entity. Indicators such as selected typical ion concentration, pH, and temperature were input into the corresponding modules of the PHREEQC software, and the uncertainty of the model was set to 0.05. The calculation results are listed in Table 3.

Table 3. Results of possible reaction equations and the simulation path.

Minerals	Possible Reaction	Mole Transfer (mmol/kg)
Anorthite	$CaAlSi_2O_8 + 1.5H_2O \rightarrow Ca^{2+} + 0.5Al_2Si_2O_5(OH)_2 + H_4SiO_4 + 2OH^-$	-2.561×10^{-3}
Gypsum	$CaSO_4 \rightarrow Ca^{2+} + SO_4^{2-}$	1.639×10^{-5}
Halite	$NaCl \rightarrow Na^+ + Cl^-$	3.324×10^{-2}
Quartz	$SiO_2 + 2H_2O \rightarrow H_4SiO_4$	-2.301×10^{-3}
Dolomite	$CaMg(CO_3)^3 + 2H_2O \rightarrow Ca^{2+}$ $+Mg^{2+} + 2HCO_3^- + 2OH^-$	5.731×10^{-4}
Illite	$KAlSi_2O_8 + 5.5H_2O \rightarrow K^+ + 0.5Al_2Si_2O_5(OH)_2$ $+3H_4SiO_4 + OH^-$	2.227×10^{-3}
Calcite	$CaCO_3 + H_2O \rightarrow Ca^{2+} + HCO_3^-$	5.896×10^{-3}
CaX_2	$CaX_2 + H_2SO_4 \rightarrow CaXO_4 + 2HX$	-2.638×10^{-3}
CO_2	/	5.073×10^{-3}

Note: Positive numbers in mole transfer indicate dissolution, while negative numbers indicate precipitation.

As revealed by the simulation results (Table 3) of the reverse hydrogeochemical reaction paths, gypsum, rock salt, calcite, dolomite, and illite all undergo dissolution reactions in the paths of the study area, and their dissolved components enter the underground

hot water, increasing the K^+, Na^+, HCO_3^-, and Cl^- concentrations. According to the geological background and lithologic characteristics of the study area, it is considered that the dissolution of minerals such as dolomite and gypsum in carbonate rocks is the main source of Sr in the geothermal fluids of the deep carbonate reservoirs.

In addition, the $^{87}Sr/^{86}Sr$ ratio of the fluids leaching through rocks of different compositions is directly related to specific rocks. The geothermal fluids in the deep thermal reservoirs of the Rongcheng geothermal field have higher $^{87}Sr/^{86}Sr$ ratios than the crust-derived Sr in carbonate rocks (global average: 0.7119) [36,37], suggesting that the Sr in the geothermal fluids may originate from crust-derived materials in addition to related mineral dissolution.

4.2.5. Estimation of the Temperature of Geothermal Reservoirs

Geothermometers are frequently used to estimate the temperature of geothermal fluids in deep reservoirs. At present, the cationic and SiO_2 geothermometers are most commonly used.

Cationic geothermometers (K–Na–Ca, K–Na, and Na–Li) are based on the association among cations [38]. Before applying a cationic geothermometer, a Na–K–Mg ternary diagram is used to determine the degree of equilibrium of the samples. If the samples are not in equilibrium (or at least partial equilibrium), cationic geothermometers cannot be applied. As shown in Figure 10, the water samples from the study area were all immature. This finding indicates that the water-rock interactions between the underground hot water and aluminum feldspar, potassium feldspar, and magnesium feldspar minerals have proceeded for a short time and have not reached the equilibrium state. Therefore, the cationic geothermometers are not suitable for this study.
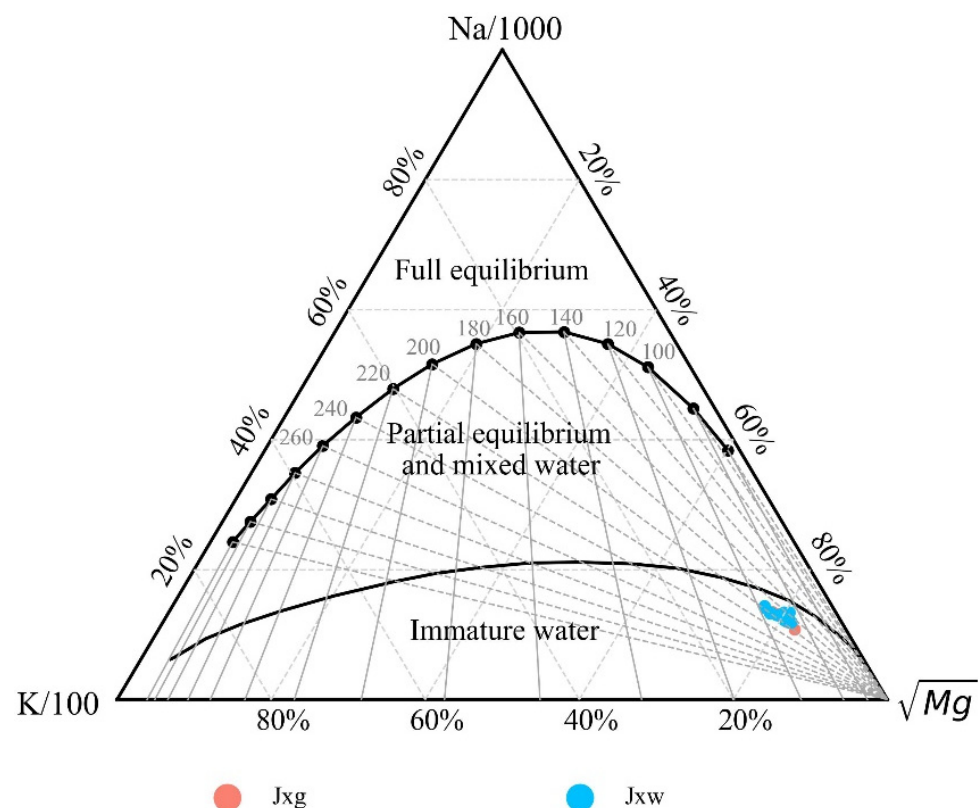

Figure 10. Na–K–Mg ternary diagram of geothermal water in the study area [38].

The SiO_2 geothermometer was developed on the basis of the solution–precipitation equilibrium theory of silica-bearing minerals in hydrothermal solution [39,40]. In other words, the solubility of SiO_2 increases with an increase in the temperature. The SiO_2

dissolved in water is not prone to be affected by the ion effect, volatilization loss, and the dilution of other complexes and is only controlled by the solubility of polycrystalline substances of silica, such as quartz. Therefore, the SiO_2 geothermometer is the most widely applied [40,41]. It can provide more reliable results than a cationic geothermometer. In this study, four SiO_2 geothermometers, namely, quartz, quartz (no steam loss), quartz (maximum steam loss), and chalcedony geothermometers (Table 4), were used to calculate the underground hot-water temperature of the deep thermal reservoirs in the study area. The chalcedony geothermometer should yield a discharge temperature of the geothermal reservoirs close to its actual value; however, the water temperatures at the locations of wells XR05 and XR08 estimated using the chalcedony geothermometer were lower than the measured temperatures, indicating that the chalcedony geothermometer yielded inaccurate results. Therefore, this study used the quartz geothermometer to estimate the average temperature of the deep thermal storage in the study area, and the estimated values were 92–113 °C (Table 5).

Table 4. Geothermometer formulas for hot water [41].

Geothermometer	Formulas
Quartz	$T(°C) = -42.198 + 0.288\,31SiO_2 - 3.6686 \times 10^{-4}\,(SiO_2)^2$ $+ 3.1665 \times 10^{-7}(SiO_2)^3 + 77.0341lgSiO_2$
Quartz (no steam loss)	$T(°C) = \frac{1309}{5.19 - lgSiO_2} - 273.15$
Quartz (maximum steam loss)	$T(°C) = \frac{1522}{5.75 - lgSiO_2} - 273.1$
Chalcedony	$T(°C) = \frac{1032}{4.69 - lgSiO_2} - 273.1$

Table 5. Estimated temperature of geothermal reservoirs in the study area (°C).

Sample No.	T	Estimated Geothermal Reservoir Temperature				
		Quartz	Quartz (No Steam Loss)	Quartz (Maximum Steam Loss)	Chalcedony	Average of Thermal Storage Temperature
XR05	62	93.18	92.69	94.71	62.18	93.53
XR06	55	91.87	91.37	93.55	60.77	92.26
XR07	68	102.45	102.05	102.81	72.19	102.44
XR08	71	100.12	99.69	100.77	69.65	100.19
XR09	55	90.94	90.44	92.75	59.78	91.38
XR11	62	98.72	98.28	99.56	68.15	98.85
XR15	56	103.71	103.31	103.90	73.55	103.64
XR16	58	98.79	98.35	99.61	68.22	98.92
XR17	71	104.23	103.84	104.36	74.12	104.15
XR19	/	101.91	101.49	102.33	71.59	101.91
XR20	64	104.53	104.15	104.62	74.45	104.44
XR21	/	113.76	113.48	112.64	84.53	113.29

5. Geological Genetic Model of the Geothermal Fluids

Owing to the breakage of the North China Craton, the lithosphere has thinned, the deep Moho has been uplifted to an average depth of 33 km, and the temperature at the bottom boundary of the upper crust has increased from 144 °C to 387 °C from the outside to the center of the basin. The measurements of heat flux in the Xiong'an New Area [42] show that the Rongcheng uplift has geothermal heat flow of 54–90 W·m^{-2}, with an average of 74.2 W·m^{-2}. As revealed by these results combined with the data on well temperature and the thermal conductivity tests of core samples [43], the Rongcheng uplift has geothermal gradients of 32–40.9 °C·km^{-1}. In addition, granulocyte basalts with a thickness of approximately 120 m are exposed at a depth of 3000 m at the location of well XR21 (D19) in the study area, which is evidence of shallow intrusions. Moreover, the geothermal fluids in the deep geothermal reservoirs in the study area have higher $^{87}Sr/^{86}Sr$ ratios than the crust-derived Sr in the carbonate rocks (global average: 0.7119). All these

findings reflect strong tectonic activities in the study area, thereby indicating a high thermal background. However, according to the theoretical calculations, the fault activities generate too little heat to serve as a heat source. Moreover, there is no residual additional heat source of magmas in the study area. Therefore, the heat from the deep mantle and the heat from the decay of radioactive elements in the upper crust constitute the heat source of the geothermal system in the study area.

After several tectonic movements in this area, a series of NNE- and NNE-trending secondary structures and large tensile faults have been formed on the Sino-Korean paraplatform and have created uplift and subsidence phases. Faults control the overall pattern of karst development and the karst paleo-landform in the study area [1,44]. The rocks on both sides of the fault zone are affected by the presence of structural fractures and intrusions. Meanwhile, diagenetic fractures develop in the fault zone and provide favorable conditions for hot water circulation. In addition, favorable factors such as fractures form reservoir space and seepage channels for thermal reservoirs. According to the analysis of hydrogeological conditions, the study area receives atmospheric precipitation, which penetrates the ground and provides a long period of lateral groundwater runoff recharge along the fault zone for the deep carbonate reservoirs. Owing to various favorable factors, the underground water rises from deep carbonate rocks after being heated through circulation convection, and the hydraulic connection between deep and shallow parts is established.

In summary, the geothermal fluids of the deep buried-hill thermal reservoirs in the study area evolve as follows: after the rainwater provides lateral runoff recharge in the northwestern Taihang Mountains followed by precipitation and infiltration, the groundwater migrates to deep strata along the fractures generated by the fault movements. Afterward, the groundwater is heated by the heat from the deep mantle and from the radioactive element decay in the upper crust and then rises along faults. With a prolonged retention time, the groundwater occurs in a closed environment. Strong water-rock interactions occur between water and related minerals such as crust-derived materials, dolomite, and gypsum, carrying crust-derived Sr and absorbing heat provided by crust-derived materials. As a result, underground hot water is formed. Along the direction of groundwater flow, the combined effects of the cumulative effect of time and rock–water interactions lead to an increase in the Sr concentration and $^{87}Sr/^{86}Sr$ ratio of the underground hot water (Figure 11).
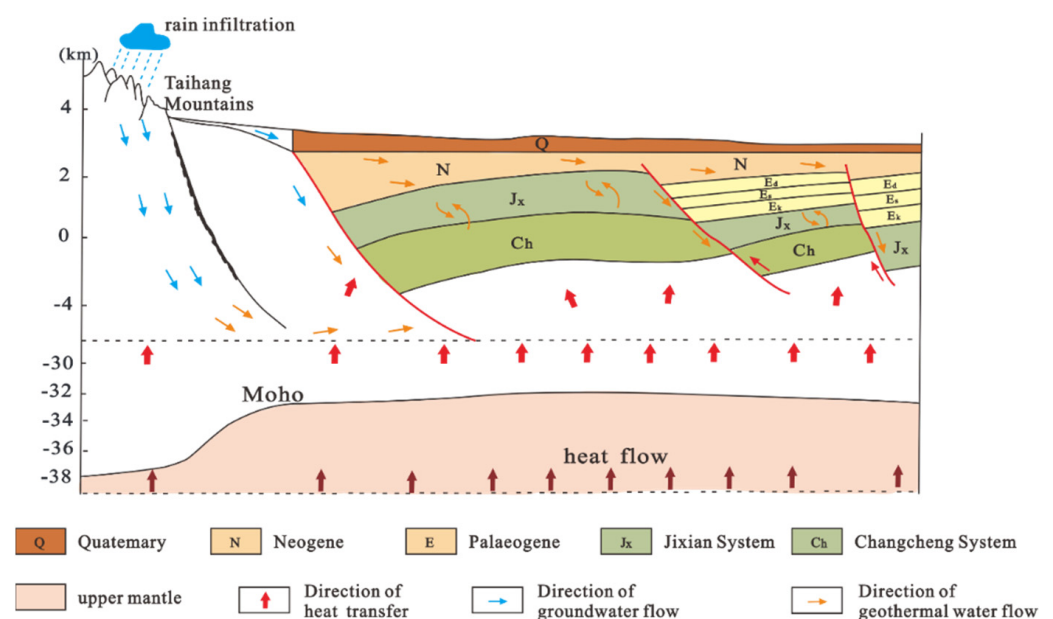

Figure 11. Geological genetic model of the geothermal water in the study area.

6. Conclusions

(1) The geothermal fluids of Jixianian carbonate reservoirs have a hydrochemical type of Cl·HCO_3-Na, pH of 7.04–8.18, and TDS content of 2445–2960 mg/L. Stable isotopes δ^2H and $\delta^{18}O$ indicate that the geothermal water of the Jixianian carbonate reservoirs is recharged by atmospheric precipitation. According to this and the relationship between isotope and hydrochemical characteristics, the geothermal water in the Jixianian carbonate geothermal reservoirs in the study area has experienced long circulation, and its storage space is relatively closed. The water-rock interactions between the geothermal water and surrounding rocks are more intense, and the contents of the hydrochemical components and TDS in the geothermal water are relatively high.

(2) ^{14}C can be used to effectively calculate the age of groundwater of the Jixianian geothermal reservoirs in the study area. According to ^{14}C dating results, the age of the geothermal water in the study area is 20–41 ka overall. In Rongcheng geothermal field, the age of the geothermal water increases from west (XR04) to east (XR15), and the water flow rate is approximately 1.02 m/a. The water in the geothermal field features slow circulation and a long runoff path, and it is characterized by deep circulating water. The formation of geothermal water is controlled by structures.

(3) Sr^{2+} and Sr isotopes can be used to effectively trace the migration path of geothermal fluids of the Jixianian geothermal reservoirs and the degree of water-rock interactions. As revealed by the simulation results of the reverse hydrogeochemical reaction paths, gypsum, rock salt, calcite, dolomite, and illite all undergo dissolution reactions in the study area, leading to an increase in the K^+, Na^+, HCO_3^-, and Cl^- concentrations. Along the groundwater flow direction, the Sr^{2+} concentration and the $^{87}Sr/^{86}Sr$ ratio in the geothermal water increase due to the dissolution of minerals such as dolomite and gypsum in carbonate rocks, as well as the cumulative effect of ages.

(4) The geothermal water of the Jixianian carbonate reservoirs in the study area is recharged by atmospheric precipitation, and their temperature is estimated to be 92–113 °C using a SiO_2 geothermometer. The geothermal fluids of the deep buried-hill thermal reservoirs in the study area evolve as follows: after the rainwater provides lateral runoff recharge in the northwestern Taihang Mountains followed by precipitation and infiltration, the groundwater migrates to deep strata along the fractures generated by fault movements. With a prolonged retention time, the groundwater occurs in a closed environment, strong water-rock interactions occur between the groundwater and related minerals such as crust-derived materials, dolomite, and gypsum, and the groundwater absorbs heat from the deep mantle and from the radioactive element decay in the upper crust, thus forming geothermal water.

Author Contributions: Conceptualization, M.Y. and G.W.; methodology, M.Y. and W.Z.; formal analysis, M.Y.; investigation, M.Y. and F.M.; resources, G.W.; data curation, M.Y.; writing—original draft preparation, M.Y. and G.W.; writing—review and editing, G.W., X.Z., W.L. and H.Z.; supervision, G.W.; project administration, G.W.; funding acquisition, G.W. and W.Z. All authors have read and agreed to the published version of the manuscript.

References

1. Wang, G.L.; Lin, W.J. Main hydro-geothermal systems and their genetic models in China. *Acta Geol.* **2020**, *94*, 1923–1937. (In Chinese)
2. Ma, B.; Jia, L.X.; Yu, Y.; Wang, H.; Chen, J.; Zhong, S.; Zhu, J.C. Geoscience and carbon Neutralization: Current status and development direction. *Geol. China* **2021**, *48*, 347–358. (In Chinese)
3. Prada, S.; Cruz, J.V.; Figueira, C. Using stable isotopes to characterize groundwater recharge sources in the volcanic island of Madeira, Portugal. *J. Hydrol.* **2016**, *536*, 409–425. [CrossRef]
4. Negrel, P.; Petelet-Giraud, E.; Millot, R. Tracing water cycle in regulated basin using stable δ^{18}O-δ^2H isotopes: The Ebro river basin (Spain). *Chem. Geol.* **2016**, *422*, 71–81. [CrossRef]
5. Huang, Q.B.; Qin, X.Q.; Liu, P.Y.; Zhang, L.K.; Su, C.T. The influence of allogenic water and sulfuric acid to karst carbon sink in karst subterranean river in southern Human. *Adv. Earth Sci.* **2017**, *32*, 102–111.
6. Yuan, R.X.; Zhang, W.; Gan, H.N.; Liu, F.; Wei, S.C.; Liu, L.X. Hydrochemical Characteristics and the Genetic Mechanism of Low–Medium Temperature Geothermal Water in the Northwestern Songliao Basin. *Water* **2022**, *14*, 2235. [CrossRef]
7. Deng, J.Z.; Lin, W.J.; Xing, L.X.; Chen, L. The estimation of geothermal reservoir temperature based on integrated multicomponent geothermometry: A case study in the Jizhong depression, North China Plain. *Water* **2022**, *14*, 2489. [CrossRef]
8. Liao, Y.Z.; Liu, Y.G.; Liu, F.; Lu, C.; Zhao, G. Genetic Mechanism of Geothermal Resources in the Qutan and Reshuizhou Geothermal Fields, Jiangxi Province, China: Evidence from Hydrogeochemical Characteristics of Geothermal Water. *Lithosphere* **2022**, *2021*, 9778217. [CrossRef]
9. Edmunds, W.M.; Smedley, P.L. Residence time indicators in groundwater: The East Midlands Triassic sandstone aquifer. *Appl. Geochem.* **2000**, *15*, 737–752. [CrossRef]
10. Yuan, L.J.; Zhang, J.P.; He, Y.C.; Kong, X.J.; Gao, J. Hydrochemical and isotopic characteristics of geothermal fluids in Tongzhou District, Beijing, and their geothermal significance. *Geol. Rev.* **2021**, *67*, 1545–1556.
11. Bozau, E.; Häußler, S.; Van Berk, W. Hydrogeochemical modelling of corrosion effects and barite scaling in deep geothermal wells of the North German Basin using PHREEQC and PHAST. *Geothermics* **2015**, *53*, 540–547. [CrossRef]
12. Chen, Z.S.; Zhu, L.J.; Liu, P.; Li, C.; Zhou, Y.N.; Li, Y.K.; Xie, H.; Xiang, T. Hydrogeochemical Evolution Mechanism of Carbonate Geothermal Water in Southwest China. *Arab. J. Geosci.* **2021**, *14*, 1310. [CrossRef]
13. Alsemgeest, J.; Auqué, L.F.; Gimeno, M.J. Verification and comparison of two thermodynamic databases through conversion to PHREEQC and multicomponent geothermometrical calculations. *Geothermics* **2021**, *91*, 102036. [CrossRef]
14. Chen, M.X. *Geothermal in North China*; Science Press: Beijing, China, 1988. (In Chinese)
15. Wang, G.L.; Zhang, W.; Liang, J.Y.; Lin, W.J.; Liu, Z.M.; Wang, W.L. Evaluation of geothermal resources potential in China. *Acta Geosci. Sin.* **2017**, *38*, 449–459. (In Chinese)
16. Wang, Y.B.; Ding, W.P.; Tian, Y.; Wang, J.; Ding, R. Genetic analysis on high-temperature geothermal water in Niutuo geothermal field. Heibei Province. *Urban Geol.* **2016**, *11*, 59–64.
17. Zhu, S.Y.; Zhang, G.B.; Li, S.H. A study on geothermal resources comprehensive utilization in Xiong'an New Area. *Coal Geol. China* **2018**, *30*, 20–23.
18. Dai, M.G.; Wang, X.W.; Liu, J.X.; Lei, H.F.; Bao, Z.D. Characteristics and influence factors of geothermal resources in the starting and adjacent zone of Xiong'an new area. *Sci. Geol. Sin.* **2019**, *54*, 176–191.
19. Wang, Y.J.; Ma, F.; Xie, H.P.; Wang, G.L.; Wang, Z.H. Fracture Characteristics and Heat Accumulation of Jixianian Carbonate Reservoirs in the Rongcheng Geothermal Field, Xiong'an New Area. *Acta Geol. Sin.-Engl. Ed.* **2021**, *95*, 1902–1914. [CrossRef]
20. Zhao, J.Y.; Zhang, W.; Ma, F.; Zhu, X.; Zhang, H.X.; Wang, G.L. Geothermal characteristics of the geothermal fluid in the Rongcheng geothermal filed, Xiong'an New Area. *Acta Geol.* **2020**, *94*, 1992–2001. (In Chinese)
21. Zhu, X.; Wang, G.L.; Wang, X.Y.; Qi, S.H.; Ma, F.; Zhang, W.; Zhang, H.X. Hydrogeochemical and Isotopic Analyses of Deep Geothermal Fluids in the Wumishan Formation in Xiong'an New Area, China. *Lithosphere* **2022**, *2021*, 2576752. [CrossRef]
22. Wang, G.L.; Li, J.; Wu, A.M.; Zhang, W.; Hu, Q.Y. A study of the thermal storage characteristics of Gaoyuzhuang Formation, A new layer system of thermal reservoir in Rongcheng uplift area, Hebei Province. *Acta Geosci. Sin.* **2018**, *39*, 533–541.
23. Hebei Regional Geological and Mineral Research Institute. *Regional Geology of China. Hebei*; Geological Publishing House: Beijing, China, 2017. (In Chinese)
24. *DZ/T 0064.64-1993*; Groundwater Test Methods. Ministry of Geology and Mineral Resources of the People's Republic of China: Beijing, China, 1993. (In Chinese)
25. *DZ/T 0184.6-1997*; Determination of Samarium-Neodymium Isotope Geological Age and Neodymium Isotope Ratio. Ministry of Geology and Mineral Resources of the People's Republic of China: Beijing, China, 1997. (In Chinese)
26. Zhang, W.; Wang, G.L.; Xing, L.X.; Li, T.X.; Zhao, J.Y. Geochemical response of deep geothermal processes in the Litang region, Western Sichuan. *Energy Explor. Exploit.* **2019**, *37*, 626–645. [CrossRef]
27. Wang, X.C.; Zhou, X. Geothermometry and Circulation Behavior of the Hot Springs in Yunlong County of Yunnan in Southwest China. *Geofluids* **2019**, *2019*, 1–16. [CrossRef]
28. Craig, H. Standard for reporting concentrations of deuterium andoxygen-18 in natural water. *Science* **1961**, *133*, 1833–1834. [CrossRef]
29. Dansgaard, W. Stable isotopes in precipitation. *Tellus* **1964**, *16*, 436–468. [CrossRef]

30. Ma, Z.Y.; Qian, H. *Environmental Isotope Groundwater Literature*; Science and Technology Publishing House: Xi'an China, 2004. (In Chinese)

31. Pearson, F.J. Use of C-13/C-12 ratios to correct radiocarbon ages of material initially diluted by limestone. In Proceeding of the 6th International Conference on Radiocarbon and Tritium Dating, Pulman, WA, USA, 7–11 June 1965; p. 357.

32. Bo, Y.; Liu, C.L.; Zhao, Y.J.; Wang, L.C. Chemical and isotopic characteristics and origin of spring waters in the Lanping–Simao Basin, Yunnan, Southwestern China. *Chem. Erde-Geochem.* **2015**, *75*, 287–300. [CrossRef]

33. Lu, L.H.; Pang, Z.H.; Kong, Y.L.; Guo, Q.; Wang, Y.C.; Xu, C.H.; Gu, W.; Zhou, L.L.; Yu, D.D. Geochemical and isotopic evidence on the recharge and circulation of geothermal water in the Tangshan Geothermal System near Nanjing, China: Implications for sustainable development. *Hydrogeol. J.* **2018**, *26*, 1705–1719. [CrossRef]

34. Gaillardet, J.; Dupre, B.; Louvat, P.; Allegre, C.J. Global silicate weathering and CO2 consumption rates deduced from the chemistry of large rivers. *Chem. Geol.* **1999**, *159*, 3–30. [CrossRef]

35. Philippe, N. Water–granite interaction: Clues from strontium, neodymium and rare earth elements in soil and waters. *Appl. Geochem.* **2006**, *21*, 1432–1454.

36. Burke, W.H.; Denison, R.E.; Hetherington, E.A.; Koepnick, R.B.; Nelson, H.F.; Otto, J.B. Variation of seawater 87Sr/86Sr throughout Phanerozoic time. *Geology* **1982**, *10*, 516–519. [CrossRef]

37. Palmer, M.R.; Elderfield, H. Sr isotope composition of sea water over the past 75 Ma. *Nature* **1985**, *314*, 526–528. [CrossRef]

38. Giggenbach, W.F. Geothermal solute equilibria. Derivation of Na-K-Mg-Ca geoindicators. *Geochim. Cosmochim. Acta* **1988**, *52*, 2749–2765. [CrossRef]

39. Morey, G.; Fournier, R.; Rowe, J. The solubility of quartz in water in the temperature interval from 25 to 300 C. *Geochim. Cosmochim. Acta* **1962**, *26*, 1029–1043. [CrossRef]

40. Fournier, R.O.; Truesdell, A.H. Geochemical indicators of subsurface temperature. Part II. Estimation of temperature and fraction of hot water mixed with cold water. *J. Res. U.S. Geol. Surv.* **1974**, *2*, 263–270.

41. Fournier, R.O. Chemical geothermometers and mixing models for geothermal systems. *Geothermics* **1977**, *5*, 41–50. [CrossRef]

42. Chang, J.; Qiu, N.S.; Zhao, X.Z.; Xu, W.; Xu, Q.C.; Jin, F.M.; Han, C.Y.; Ma, X.F.; Dong, X.Y. Present-day geothermal regime of the Jizhong depression on Bohai Bay basin, East China. *Chin. J. Geophys.* **2016**, *59*, 1003–1016. (In Chinese)

43. Wang, Z.T.; Zhang, C.; Jiang, G.Z.; Hu, J.; Tang, X.C.; Hu, S.B. Present-day geothermal field of Xiongan New Area and its heat source mechanism. *Chin. J. Geophys.* **2019**, *62*, 4313–4322. (In Chinese)

44. Lin, W.J.; Wang, G.L.; Gan, H.N.; Zhang, S.S.; Zhao, Z.; Yue, G.F.; Long, X.T. Heat source model for Enhanced Geothermal Systems (EGS) under different geological conditions in China. *Gondwana Res.* **2022**, *in press*.